The 2009 IEEE/RSJ International Conference on
Intelligent Robots and Systems
October 11-15, 2009 St. Louis, USA

Design Optimization of a Delta-Like Parallel Robot through Global Stiffness Performance Evaluation

Eric Courteille, Dominique Deblaise, Patrick Maurine

Abstract— **This paper presents the design optimization of a Delta-like robot manipulator with respect to multiple global stiffness objectives. For this purpose, a systematic elasto-geometrical modeling method is used to derive the analytical manipulator stiffness models by taking into account their link and joint compliances. The models are then involved within a statistically sensitivity analysis of the influence of the geometric parameters on four global indices that describe the structure stiffness over the workspace. Multi-Objective Genetic Algorithm, i.e. Pareto-optimization, is taken as the appropriate framework for the definition and the solution of the addressed multi-objective optimization problem. Our approach is original in the sense that it is systematic and it can be applied to any serial and parallel manipulators for which stiffness is a critical issue.**

I. Introduction

The main objective for the mechanical design of robot manipulators consists in finding the best compromise between several properties, such as workspace, dexterity, manipulability, and stiffness [1]. Stiffness is an important issue for serial and parallel robots manipulators since their structures are now gradually being implemented to carry out various applications in fields such as medical, flight simulation and high-speed machining [2]. To make these machines compatible with their applications, it is necessary to model, identify and compensate all the effects that degrade their accuracy. These effects may be caused by errors in the geometry tolerances of the structure associated with machining and assembly errors of the various constituting bodies, and also by the elastic deformations of their structures [3], [4], [5], [6]. The main problem is that a low stiffness of links and/or joints may lead to large compliant displacements of the end-effector under both structure own weight and external wrench applied at the end-effector [7]. These compliant displacements detrimentally affect both accuracy and payload performances, as pointed out for example in [8]. It is also to be noted that insufficient stiffness may induce low natural frequencies of the structure that lead to longer stabilization times and reduced dynamic performances [9].

In the literature many efforts were recently devoted to the design optimization of robot manipulators by considering many competing objectives such as velocity transmission, workspace, inertia and stiffness [10], [11], [12]. These studies have shown the real efficiency of the evolutionary algorithms to solve this kind of problems. However, most of them do not include a parametric stiffness analysis of the optimization problem as part of the design process.

It is in this context that the presented work takes place. Our main objective is to fulfill the industrial demands in the preliminary design of the robots manipulators by optimizing simultaneously the stiffness over a specific workspace and/or by minimizing the global weight of the structure for increased dynamic performances, the whole in an acceptable timeframe. The main originality of our work resides:

- in a systematic analytical calculation of the equivalent stiffness matrix of the manipulator structures through a method that we already proposed and experimentally validated in [13], [6],
- in the use of realistic global stiffness indices derived from the concatenation of the equivalent stiffness matrices locally calculated in the manipulator workvolume [14], [7],
- in a statistical sensibility analysis based on the t-Student parameter [15] to find out the most important design parameters in the optimization problem,
- in the fact to provide an interactive use of Multi-Objective Genetic Algorithms (MOGA) in the robot design optimization as a reliable tool from an engineer point of view.

The paper is organized as follows. The stiffness modeling of a 3 degree-of-freedom translational parallel manipulator that is used to illustrate the proposed method is described first. The definition of local stiffness performance indices is done next. Global performance indices are then proposed and a sensibility analysis is done using the t-Student method. Then a practical application of the multi-objective optimization procedure is presented in order to define optimal stiffness designs of a Delta-like structure for which the optimization results are carefully analyzed.

II. Stiffness modeling of a Delta-like mechanism

The Surgiscope®[1] is a hybrid structure with a position mechanism based on a Delta-like parallel manipulator [16] and a decoupled orientation mechanism. This structure is used in neurosurgery to move and to place accurately a microscope, a laser guiding system and some others surgical tools. In the following, the Surgiscope will only designate the position mechanism (Fig. 1).

E. Courteille, D. Deblaise, P. Maurine, are with the LGCGM (EA 3913), Rennes, France and with the Department of Mechanical and Control Systems Engineering, INSA de Rennes, France
eric.courteille@insa-rennes.fr
dominique.deblaise@insa-rennes.fr
patrick.maurine@insa-rennes.fr

[1]ISIS: Intelligent Surgical Instrument & Systems http://www.isis-robotics.com/

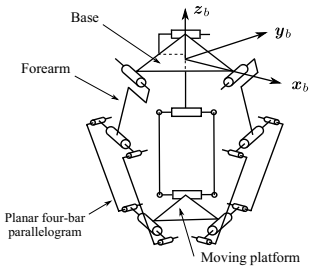

Fig. 1. The Surgiscope.

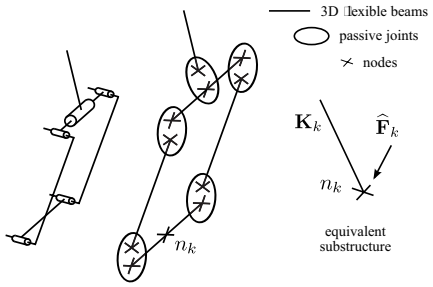

Fig. 2. Modeling of the k^{th} kinematic chain.

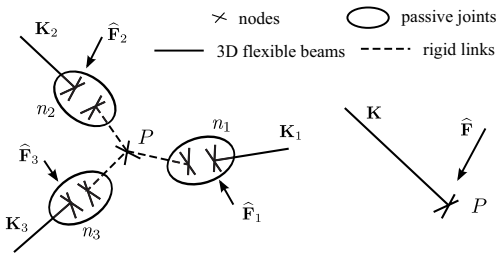

Fig. 3. Modeling of the equivalent structure.

The analytical stiffness model presented in this section is based on matrix structural analysis and has been introduced in previous papers [6], [13]. Compared to traditional CAD-FEA approach, this analytical modeling leads both to a realistic stiffness description as well as a reduction of computational time that allows its use in a parametric optimization loop.

The stiffness modeling of the Surgiscope is composed with nodes corresponding to the characteristic points. These nodes link some 3D flexible beams, some rigid elements and some joints. The 6 dimensional equivalent stiffness matrix $\mathbf{K}$ of the Surgiscope is defined in two steps as follows:

- definition of the equivalent substructure of each kinematic chain k ($k = 1, 2, 3$) defined by the equivalent stiffness matrix $\mathbf{K}_k$ and the equivalent external wrench (force/torque) $\widehat{\mathbf{F}}_k$ (Fig.2);
- assembly of the three equivalent kinematic chains to the moving platform considered as rigid. Definition of the equivalent structure defined by the stiffness matrix $\mathbf{K}$ or the compliance matrix $\mathbf{C} = \mathbf{K}^{-1}$ and the equivalent external wrench $\widehat{\mathbf{F}} = \left[\begin{array}{cc} \mathbf{f}^T & \tau^T \end{array} \right]^T$ acting at the center point of the moving platform (Fig. 3) and that produces its elastic displacements given by the twist (linear/rotational deformations) $\widehat{\mathbf{X}} = \left[\begin{array}{cc} \mathbf{d}^T & \gamma^T \end{array} \right]^T$.

As a result, this modeling phase leads to the stiffness and compliance mapping relations:

$$\widehat{\mathbf{F}} = \mathbf{K}\widehat{\mathbf{X}}, \qquad \widehat{\mathbf{X}} = \mathbf{C}\widehat{\mathbf{F}}. \tag{1}$$

Table I shows the parameters, the boundaries and the nominal values of the Surgiscope. Note that the genetic algorithm used as optimization scheduler will impose to consider the individual parameters such as discrete variables. The steps are defined by nearly respecting the manufacturing tolerances in order to not increase artificially the research space. The generated solutions thereafter will largely depend on the boundaries and the steps chosen since they define the nature and the dimensions of the research space.

III. Stiffness performance evaluation

Since it has been shown in the previous part that the configuration-dependent Cartesian stiffness and compliance matrices $\mathbf{K}$ and $\mathbf{C}$ can be obtained analytically for a joint configuration $\mathbf{q}$, the stiffness performance of robot manipulators can be studied in a systematic way through the proposition of some relevant indices.

Due to the fact that stiffness and compliance mappings are described by tensorial quantities, there is no obvious way to give a quantification of the mechanism behavior such as a stiffness constant of a linear spring for example [17]. One solution consists in separating the quantity into geometric contents such as eigenvalue problems. However, the eigenvalue problem of equation (2) cannot be solved by using the spatial stiffness matrix $\mathbf{K}$ since the eigenvalues λ do not have a physically consistent unit and are not invariant under a coordinate transformation [18].

$$\mathbf{K}\widehat{\mathbf{X}} = \lambda\widehat{\mathbf{X}} \tag{2}$$

TABLE I
Design parameters values

Parameters (Unit)	Description	Nominal value	Lower bound	Upper bound	Step
$L_1\ (m)$	Forearm length	0.75	0.7	0.8	$1e^{-3}$
$L_2\ (m)$	Parallelogram length (long side)	0.95	0.85	1.05	$1e^{-3}$
$L_3\ (m)$	Parallelogram length (small side)	0.125	0.1	0.15	$1e^{-3}$
$T_1\ (mm)$	Forearm thickness	2	2	10	0.5
$T_2\ (mm)$	Parallelogram thickness	5	2	10	0.5
$\phi_1\ (mm)$	Forearm diameter	70	50	100	0.5
$\phi_2\ (mm)$	Parallelogram diameter (long side)	25	15	60	0.5
$\phi_3\ (mm)$	Parallelogram diameter (small side)	22	10	40	0.5
$R_n\ (m)$	Moving platform radius	0.2	0.15	0.25	$1e^{-3}$

In order to overcome this unit inconsistency and coordinate transformation dependance, the approach that is used in this paper is to solve the alternative eigenvalue problem proposed by Lipkin and Patterson [19] that is reminded hereafter. Its formulation comes from the minimization of the potential energy storage of the manipulator mechanism (initially in a stable potential field) when a wrench applied on the Tool Center Point (TCP) induces an elastic displacement twist. For a unit magnitude wrench or twist, the two minimization problems that are to be solved are:

$$\begin{aligned} &\text{minimize :} \quad w_1 = \tfrac{1}{2}\widehat{\mathbf{F}}^T\mathbf{C}\widehat{\mathbf{F}} \\ &\text{subject to :} \quad \widehat{\mathbf{F}}^T\mathbf{\Gamma}\widehat{\mathbf{F}} = 1 \end{aligned} \tag{3}$$

and

$$\begin{aligned} &\text{minimize :} \quad w_2 = \tfrac{1}{2}\widehat{\mathbf{X}}^T\mathbf{K}\widehat{\mathbf{X}} \\ &\text{subject to :} \quad \widehat{\mathbf{X}}^T\mathbf{\Omega}\widehat{\mathbf{X}} = 1 \end{aligned} \tag{4}$$

with : $\mathbf{\Gamma} = \begin{bmatrix} \mathbf{I}_3 & \mathbf{0}_3 \\ \mathbf{0}_3 & \mathbf{0}_3 \end{bmatrix}$ and $\mathbf{\Omega} = \begin{bmatrix} \mathbf{0}_3 & \mathbf{0}_3 \\ \mathbf{0}_3 & \mathbf{I}_3 \end{bmatrix}$.

This leads to the two generalized singular eigenvalue problems given by:

$$\mathbf{c}_f\mathbf{\Gamma}\widehat{\mathbf{F}} = \mathbf{C}\widehat{\mathbf{F}}, \qquad \mathbf{k}_\gamma\mathbf{\Omega}\widehat{\mathbf{X}} = \mathbf{K}\widehat{\mathbf{X}} \tag{5}$$

where the eigenvalues $\mathbf{c}_f$ and $\mathbf{k}_\gamma$ correspond to the respective Lagrange multipliers involved to solve the optimization problems (3) and (4). By using the fact that $\mathbf{C} = \mathbf{K}^{-1}$, equations (5) can be rewritten as follows:

$$\mathbf{k}_f\widehat{\mathbf{F}} = \mathbf{K}\mathbf{\Gamma}\widehat{\mathbf{F}}, \qquad \mathbf{c}_\gamma\widehat{\mathbf{X}} = \mathbf{C}\mathbf{\Omega}\widehat{\mathbf{X}} \tag{6}$$

where $\mathbf{k}_f = \dfrac{1}{\mathbf{c}_f}$ and $\mathbf{c}_\gamma = \dfrac{1}{\mathbf{k}_\gamma}$. Note that this eigenvalue problem formulation is always possible since the matrix $\mathbf{K}$ ($\mathbf{C}$) is positive semi-definite [19].

Solutions of the equation system (6) under the constraints respectively $\widehat{\mathbf{F}}^T\mathbf{\Gamma}\widehat{\mathbf{F}} = 1$ and $\widehat{\mathbf{X}}^T\mathbf{\Omega}\widehat{\mathbf{X}} = 1$ are:

$$\begin{aligned} \widehat{\mathbf{F}}_{f,j} &= \begin{bmatrix} \mathbf{f}_j \\ \tau_j \end{bmatrix}, \widehat{\mathbf{X}}_{f,j} = \begin{bmatrix} c_{f,j}\mathbf{f}_j \\ \mathbf{0}_{3,1} \end{bmatrix}, \mathrm{j} = 1,2,3 \\ \widehat{\mathbf{X}}_{\gamma,j} &= \begin{bmatrix} \delta_j \\ \gamma_j \end{bmatrix}, \widehat{\mathbf{F}}_{\gamma,j} = \begin{bmatrix} \mathbf{0}_{3,1} \\ k_{\gamma,j}\gamma_j \end{bmatrix}, \mathrm{j} = 1,2,3 \end{aligned} \tag{7}$$

The resulting wrenches $\widehat{\mathbf{F}}_{f,j}$ ($\mathrm{j} = 1,2,3$) that cause only pure translation displacements parallel to the force parts are called an eigenwrenches (or wrench-compliant axes). In a similar way, the twists $\widehat{\mathbf{X}}_{\gamma,j}$ that produce only pure couples parallel to the rotation parts are named the eigentwists (or twist-compliant axes).

As a result, the first equation of (5) yields to the definition of the linear compliance ellipsoid for which the resulting translational elastic displacements are parallel to the wrenches only along the ellipsoid axes (Fig. 4). And in meantime the second equation leads to the definition of the angular stiffness ellipsoid for which the couples are parallel to the twist only along the ellipsoid axes (Fig. 5). Those ellipsoids have no dedicated location in space since the resulting translational displacements and couples are free vectors.

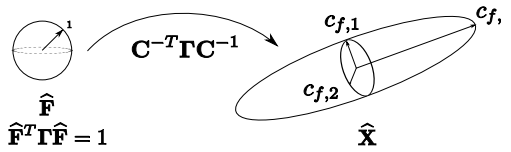

Fig. 4. Linear compliance ellipsoid.

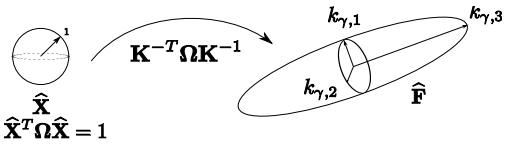

Fig. 5. Angular stiffness ellipsoid.

In the following, based on the geometrical properties of those ellipsoids some indices are proposed to evaluate the stiffness of the manipulator. Since the equation system (5) can be rewritten as (6), four local and global indexes are proposed through the study of the matrices $\tilde{\mathbf{K}} = \mathbf{K}\mathbf{\Gamma}$ and $\tilde{\mathbf{C}} = \mathbf{C}\mathbf{\Omega}$ in order to describe the stiffness for a manipulator given configuration in space and in its overall workspace.

A. Local stiffness indices

1) Condition number of $\tilde{\mathbf{K}}$ and $\tilde{\mathbf{C}}$: Two first possible indices are respectively the condition numbers $S_{k1,i}$ and $S_{c1,i}$ of the stiffness and compliance matrices $\tilde{\mathbf{K}}$ and $\tilde{\mathbf{C}}$ given by the ratio of their maximum and minimum eigenvalues:

$$S_{k1,i} = \frac{k_{f\,\max,i}}{k_{f\,\min,i}}, \quad S_{c1,i} = \frac{c_{\gamma\,\max,i}}{c_{\gamma\,\min,i}}. \tag{8}$$

Geometrically, the ratios $S_{k1,i}$ and $S_{c1,i}$ give an indication of the excentricity of the linear stiffness and angular compliance ellipsoids. For minimum values of $S_{k1,i}$ and $S_{c1,i}$ that is to say for values near to 1, those ellipsoids are closer to a sphere. As a result, minimizing those indices allows to avoid for a manipulator configuration i a sharp linear stiffness and angular compliance ellipsoids for which, the manipulator would have a high stiffness along a given axis and a low stiffness along another.

2) Minimum eigenvalue of $\tilde{\mathbf{K}}$ and maximum eigenvalue of $\tilde{\mathbf{C}}$: Two other possible indices are defined as:

$$S_{k2,i} = k_{f\,\min,i}, \quad S_{c2,i} = c_{\gamma\,\max,i}. \tag{9}$$

From a geometrical point of view, the index $S_{k2,i}$ conveys the idea that for the configuration i, the shortest axis of the linear stiffness ellipsoid should be as long as possible and on the contrary for the index $S_{c2,i}$, the longest axis of the angular compliance ellipsoid should be as short as possible.

B. Global stiffness indices

Based upon the previously defined local indices, the four global stiffness indices that will be used further for the optimal design of manipulators are defined in an original manner. For this purpose, the manipulator workspace is as usual discretized by using a regular space grid and for each equally spaced node N_i of the grid ($i = 1, ..., n_N$), the stiffness and compliance matrices $\tilde{\mathbf{K}}_i$ and $\tilde{\mathbf{C}}_i$ are calculted. Then the global equivalent stiffness and compliance matrices $\tilde{\mathbf{K}}^G$ and $\tilde{\mathbf{C}}^G$ are defined by the concatenation of all the n_N matrices $\tilde{\mathbf{K}}$ and $\tilde{\mathbf{C}}$ as follows:

$$\tilde{\mathbf{K}}^G = \begin{bmatrix} \tilde{\mathbf{K}}_1 \\ \tilde{\mathbf{K}}_2 \\ \vdots \\ \tilde{\mathbf{K}}_{n_N} \end{bmatrix}_{(6n_N \times 6)} ; \quad \tilde{\mathbf{C}}^G = \begin{bmatrix} \tilde{\mathbf{C}}_1 \\ \tilde{\mathbf{C}}_2 \\ \vdots \\ \tilde{\mathbf{C}}_{n_N} \end{bmatrix}_{(6n_N \times 6)} . \tag{10}$$

In the following, based on the fact that eigenvalue problem (6) is coordinate frame invariant, four global indices are proposed as explained by using the Singular Value Decomposition (SVD) of the global linear stiffness and angular compliance matrices $\tilde{\mathbf{K}}^G$ and $\tilde{\mathbf{C}}^G$:

$$\tilde{\mathbf{K}}^G = \mathbf{U}_f^G \mathbf{\Sigma}_f^G \mathbf{V}_f^{G^T}, \quad \tilde{\mathbf{C}}^G = \mathbf{U}_\gamma^G \mathbf{\Sigma}_\gamma^G \mathbf{V}_\gamma^{G^T} \tag{11}$$

where $\mathbf{\Sigma}_f^G = diag(\sigma_1^f, \sigma_2^f, \sigma_3^f, 0, 0, 0)$ with $(\sigma_1^f > \sigma_2^f > \sigma_3^f > 0)$ and $\mathbf{\Sigma}_\gamma^G = diag(\sigma_1^\gamma, \sigma_2^\gamma, \sigma_3^\gamma, 0, 0, 0)$ with $(\sigma_1^\gamma > \sigma_2^\gamma > \sigma_3^\gamma > 0)$.

1) Condition number of the global stiffness and compliance matrices: The global indices S_{k1} and S_{c1} give an indication of the eccentricities of the global linear stiffness and angular compliance ellipsoids which have to be minimized overall the manipulator workspace. Their values are calculated as follows:

$$S_{k1} = \frac{\sigma_1^f}{\sigma_3^f}, \quad S_{c1} = \frac{\sigma_1^\gamma}{\sigma_3^\gamma}. \tag{12}$$

2) Minimum singular value of $\tilde{\mathbf{K}}^G$ and maximum singular value of $\tilde{\mathbf{C}}^G$: The global indices S_{k2} and S_{c2} concern the length of the smallest semiaxis of the global linear stiffness ellipsoid which has to be maximized and the length of the longest semiaxis of the global angular compliance ellipsoid which has to be minimized:

$$S_{k2} = \sigma_3^f, \quad S_{c2} = \sigma_1^\gamma. \tag{13}$$

IV. Surgiscope stiffness analysis

A. Calculation of the global stiffness indices of the Surgiscope

For the calculation of all indices, the workspace is discretized by using a regular spatial grid included in a singularity free area of the Surgiscope [20]. This grid is made of some parallel and horizontal planar grids defined within a volume described by $-0.3\,m \leq X \leq 0.3\,m$, $-0.3\,m \leq Y \leq 0.3\,m$ and $-1.4\,m \leq Z \leq -0.9\,m$. In an attempt to solve the optimization problem in an acceptable timeframe while maintaining a smooth variation of the local stiffness indices from one node to the nodes that it is connected with, a number $n_N = 294$ nodes are regularly fixed over the Surgiscope workspace. This includes 6 planes of 49 nodes each. For all nodes, the linear stiffness and angular compliance matrices $\tilde{\mathbf{K}}_i$ and $\tilde{\mathbf{C}}_i$ are calculated in order to derive the global S_{k1}, S_{c1}, S_{k2}, S_{c2} indices previously defined. Based upon this calculation, a study of the influence of the Delta geometrical parameter variations onto the Surgiscope global stiffness is done.

B. Influence of the Surgiscope geometrical parameter variations onto the stiffness global indices

The main purpose of this part is to study the influence of the variations of the Surgiscope geometrical parameters onto its global stiffness S_{k1}, S_{c1}, S_{k2}, S_{c2}. This allows to verify that the variations of the global stiffness indices can describe the effects of the variations of the Surgiscope geometrical parameters. For this analysis, the spatial grid described in IV-A is used to calculate the global stiffness indices under the variations of the parameters given Table I.

1) Simultaneous variation of two geometrical parameters: For example, the Fig. 6 gives the results obtained for the simultaneous variations of the arm length L_1 and parallelogram small side bar diameter ϕ_3 which values increase respectively from 0.7 to $0.8\,m$ and from 0.01 to $0.04\,m$. As one can see, the global stiffness of the Surgiscope logically goes up for increasing values of ϕ_3 when in the meantime it remains stable when the arm length L_1 varies. On the contrary, the excentricity of the global linear stiffness and angular compliance ellipsoids are only sensitive to the variation parameter L_1. As one can see, such parametric analyze is interesting at a pre-design stage to study the effects of one or two geometrical parameters onto the global stiffness of the Surgiscope. However, this analyze is limited since it is difficult to have a global overview of the combined effects of all geometrical parameters [21]. A solution of this problem is to achieve a sensibility analysis using the t-Student method.

2) t-Student test: For the sensibility analysis of the geometrical parameters onto the global stiffness of the Surgiscope, the t-Student method provided by the optimization program modeFRONTIER was used [15]. By this method, it is possible to determine statistically if there is a relationship between the global stiffness indices and the Surgiscope geometrical parameters. Fig. 7 and 8 show the t-Student analysis diagrams.

The t-Student test compares the difference between the means of two samples of designs taken randomly in the design space:

- M_+ is the mean of the n_+ values for an objective S in the upper part of domain of the input variable,
- M_- is the mean of the n_- values for an objective S in the lower part of domain of the input variable.

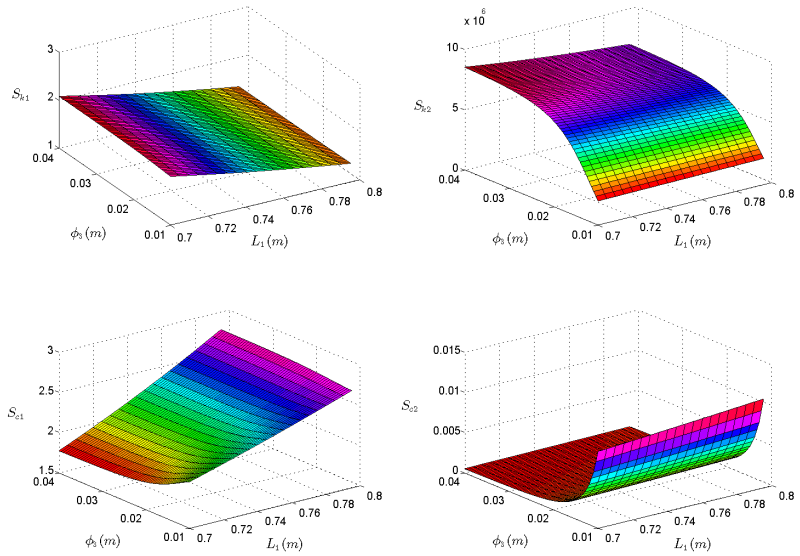

Fig. 6. Evolution of the global stiffness indices S_{k1}, S_{c1}, S_{k2}, S_{c2} under a simultaneous variations of the geometrical parameters L_1 and ϕ_3.

The t-Score for an input variable is defined according to the formula:

$$t = \frac{|M_- - M_+|}{\sqrt{\frac{V_G^2}{n_-} + \frac{V_G^2}{n_+}}} \tag{14}$$

where:

- $V_G^2 = \dfrac{(n_- - 1)V_-^2 + (n_+ - 1)V_+^2}{(n_+ + n_- - 2)}$ is the general variance,
- $V_+^2 = \dfrac{\sum(S_+ - M_+)^2}{(n_+ - 1)}$ is the variance of the population for the objective S in the upper part of the domain of the input variable,
- $V_-^2 = \dfrac{\sum(S_- - M_-)^2}{(n_- - 1)}$ is the variance of the population for the objective S in the lower part of the domain of the input variable,

The Effect parameter, expressed as a percentage of the maximum absolute value of all differences between M_- and M_+, shows how strong is the relationship between an objective and an input parameter. An Effect value greater than zero attests a direct relationship with the input variable, a value less than zero indicates that the relationship is inverse. For this reason, this parameter creates a ranked list of important factors. Low values indicate that there is no relationship between input and output variables so, probably, it is possible to ignore that variable in the optimization loop.

Another important parameter, the Significance, is calculated based on the value of t-Score (14) and the comparison of this value with a built-in table that determines the confidence level on the hypothesis that the mean values of the two samples are the same. Low value of Significance parameter indicates that the previous result (the value of Effect) is probably true. Consequently, a low value of significance does not necessarily mean that the input is highly important, but that the effect parameter is probably reliable. In fact, t-Student method is helpful only with well-sized data sets. With low sampling information tend to be unusable.

All the following statistical consideration has been taken by the comparison of 2000 designs generated by a quasi-random sequence (SOBOL algorithm), filling in a uniform manner the design space given in Table I.

Fig. 7 and 8 show that the relationships are more reliable in the diagram S_{c1} than in the others. In fact, all the design variables have a Significance value near zero in the S_{c1} diagram except the variable L_3. In the S_{k1} diagram 5 variables have no reliable relationships (ϕ_1, ϕ_2, T_1, T_1, and L_3). An explanation possible is that the S_{k1} indice was more non-linear than the others and/or the size of the data set was not big enough to describe it.

Another interesting observation that can be done from Fig. 7 and 8 concerns the direction of the relationships. In fact, there are many variables that have opposite effects on the stiffness performance values. We can see for example that the relationship between the L_1 variable and the performance indice S_{k1} that is to be minimized is very reliable and strong. On the other hand, the relationship between that variable and the performance indice S_{c1}, which also is to be minimized, is inverse and quite as reliable. The conflict between the two indices S_{k1} and S_{c1} and the uncertainty of the S_{k1} indice

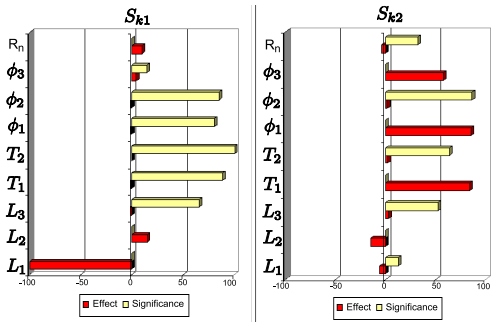

Fig. 7. T-Student diagrams for S_{k1} and S_{k2}.

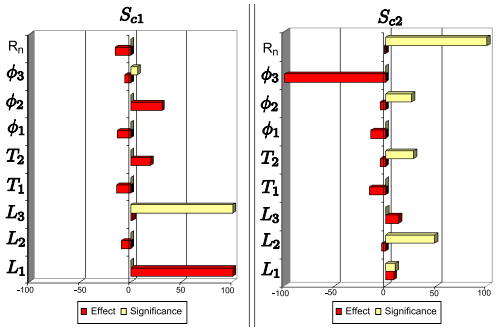

Fig. 8. T-Student diagrams for S_{c1} and S_{c2}.

will reduce the possibility of finding solutions which result in extreme improvements on these objectives.

V. Design Optimization of the Surgiscope

A. Problem formulation

The optimization program FRONTIER and the technical computing software MATLAB® are used to set up the framework of the multi-objective design optimization study of the Surgiscope. As emphasized below, an optimal stiffness design of a robot manipulator can only be achieved by considering four global indices over the workspace. The objective of the optimization is to maximize S_{k2} while simultaneously minimizing S_{k1}, S_{c1} and S_{c2}. With reference to the Surgiscope mechanism under investigation, 9 design variables are tuned (Table. I). In addition to these main performances indices, a constraint on the mass is to be set. The mass of the Surgiscope must not exceed the nominal threshold value of 21 kg. An indirect geometrical constraint is that all designs whose workspace does not include the nominal workspace defined in IV-A are automatically considered as invalid and excluded from the optimization flow.

1) Global optimization process: The Multi-objective Genetic Algorithm (MOGA), implemented first by Fonseca and Fleming [22], is used to perform the optimization problem. The algorithm will attempt a number of evaluations equal to the size of the initial population for the MOGA multiplied by the number of generation. A rule of thumb would suggest possibly to accumulate an initial population possibly more than $2 * number\ of\ variables * (number\ of\ objectives + number\ of\ constraints)$. Thus, the initial population is generated by a random sequence of 90 designs (9 design variables, 4 objectives, 1 constraint).

The major disadvantage of the MOGA is mainly related to the number of evaluations necessary to obtain satisfactory solutions. The search for the optimal solutions extends in all the directions from design space and produces a rich data base and there is not a true stop criterion. But the uniformity and the richness of the data base are very useful for the capitalization and the statistical analysis of the results. In the context of pre-stage design, the numerical evaluation of the performances calls upon MATLAB codes is not so expensive in terms of computing time (about 8 s). In an attempt to solve the optimization problem in an acceptable timeframe, the number of generations evaluated is almost 30, i.e. 2770 designs in all. The required computation time for the global optimization process is about 6 hours (2.0 GHz / 2.0 Gb RAM). Integrating a Response Surface Methodology to reduce the computation time could be an interesting extension of our work.

B. Numerical Results

1) Algorithm convergence: Fig. 9 highlights the MOGA convergence toward the maximization of the global index S_{k2}. Of the 2770 designs analyzed, 8 generate an error since they do not respect the required workspace, and 565 are unfeasible designs since they do not respect the mass constraint fixed at 21 kg. These unfeasible designs are represented with a grey rhomb on Fig. 9. In spite of an initial population largely dominated by individuals exceeding the mass constraint, the algorithm allows a good and rather fast convergence.

Fig. 10 shows the projection of the resulting Pareto-optimal sets onto the S_{k2}/S_{c2} domain, stressing the improvement that can be obtained for the two objectives respecting the mass constraint. The most interesting characteristic of this figure is the shape of the Pareto-front on these objectives. The Pareto-front is very wide. The two indices are conflicting as it was suggested by the t-Student diagrams analysis (Fig. 7 and 8). The influence of ϕ_3 is important and opposite for these two objectives. The left-up region of the Fig. 10 is characterized by a non-feasibility against the mass constraint.

2) Tradeoffs decision using multiple criteria: By definition, the MOGA will articulate design preference information after generating solutions. The MOGA defines a *posteriori* method which generates a set of solutions, with the decision marker's selecting a preferred solution afterwards. They can be regarded as a means of generating information for the user to base preference information on.

If the number of solutions is large, it will not even be obvious which of the designs are Pareto-optimal with respect to this particular set. So a filter needs to be provided to identify the non-dominated members of the set. These can then be listed numerically or displayed graphically. Various methods have been used to display sets of solutions in a multiple dimensional objective space. When there are many

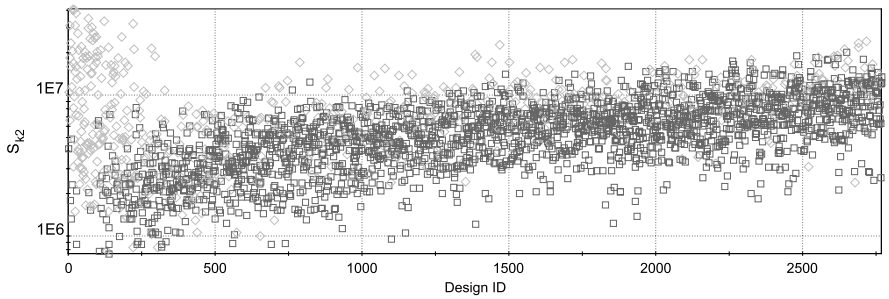

Fig. 9. Iteration history of S_{k2}.

objectives and constraints, a main diagrammatic tool to assist understanding is parallel coordinates [23]. The selection of the optimal structure inside the Pareto-set designs can be done easily by using an interactive filter on the parallel coordinates chart of the global stiffness indices and the mass constraint (Fig. 11). The design engineer balances these factors off against each others to arrive at what he thinks is the best combination of properties in the final design. There is no a unique solution. It is clear that in broad terms design is a creative process involving the use of knowledge and experience of the designer.

3) Optimal stiffness design: Of the 2770 designs analyzed, 269 were Pareto-optimal with respect to the others. Of these, the design ID 2667 is identified as being a good candidate for best overall design. The improvement of the optimal stiffness solution with respect to the nominal design is discussed in detail and shown in Table. II. The comparison of the stiffness performances of the candidate optimal solution with those of the nominal structure stresses the sensible improvement that can be obtained for all the objectives with an identical mass. The average improvement on the global stiffness performance indices S_{k2} and S_{c2} is about 30% while the performance indices S_{k1} and S_{c1} prove to be 12% better than the corresponding of the reference structure. Maybe the weak relationship between geometrical parameters and objectives characterizing the excentricity of the stiffness hyperellipsoid reduces the possibility of finding solutions which result in extreme improvements on performance indices S_{k1} and S_{c1}. For this reason, the indices S_{k1} and S_{c1} were not judged completely satisfactory and can be replaced by simple constraints fixed by the nominal design. The geometrical modifications obtained for the optimal design ID 2667 confirm the conclusions advanced in IV-B (Table. III). The optimal values stay closed to the initial ones since the optimization is done under the constraint that the initial workspace remains always reachable.

In order to show the stiffness improvement, we have computed the value of the maximal and the mean of the resulting TCP elastic displacements for a payload of $800\,N$ (Table. IV). By considering the optimal stiffness design ID 2667, the improvement is about 45% on the mean as on the max of the resulting TCP elastic displacement δz_i. The angular deflections are also optimized in almost the same proportion that those in translation for the design ID 2667 (Table. IV). Fig. 12 illustrates the distribution of the resulting TCP elastic displacements δz_i at the altitude $Z = -1.2m$ for the optimal and nominal designs. It can be observed that the improvement obtained for the design ID 2667 is uniformed all over the workspace, and one can note that the excentricity is also reduced.

4) Optimal weight design: The search for the optimal stiffness provides solutions that preserve identical stiffness properties to the nominal design, while minimizing the mass. The design ID 2430 performs a reduction of almost 25% on the mass while conserving, or even while improving global stiffness indices (Table. II).

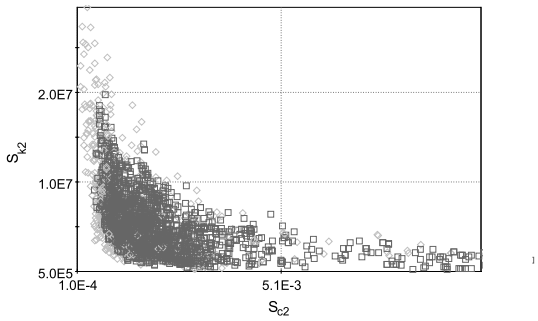

Fig. 10. Scatter chart of S_{k1} versus S_{k2}.

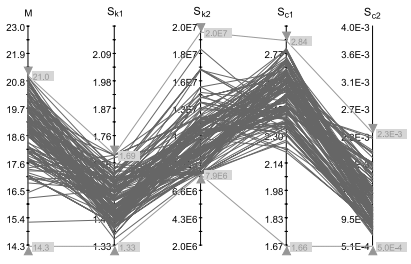

Fig. 11. Parallel coordinates chart of the Pareto-optimal designs.

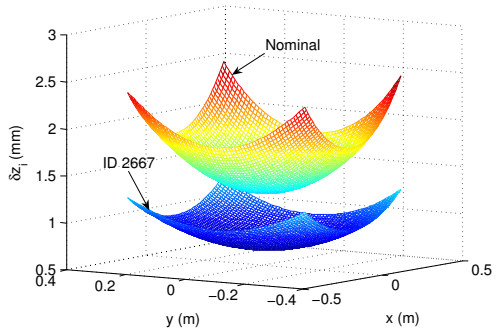

Fig. 12. δz_i for a 625 node planar grid set at the altitude $Z = -1.2\,m$.

VI. Conclusion

Design optimization of robots manipulators must be done in a short period of time and, as a result, an automated procedure for finding an optimum stiffness structure is proposed. The presented optimization, based on an original and systematic elasto-geometrical modeling, fulfills the industrial demands in the preliminary design of the robot manipulators: optimizing simultaneously the stiffness over a specific workspace and minimizing the global weight of the structure for dynamic performances increased, the whole in an acceptable timeframe. The interactive use of evolutionary multi-objective algorithm in the robot design optimization is very attractive from the engineering viewpoint. Pareto-optimization may be considered as a tool providing a set of efficient solutions among different and conflicting objectives, under different constraints. The final choice remains always subjective and is left to the designer responsibility.

References

[1] L.W. Tsai. *Robot analysis: The mechanics of serial and parallel manipulators*. New York: Wiley, 1999.

TABLE II

Evaluation global stiffness indices for the Surgiscope

Design	Mass (kg)	S_{k1}	S_{k2}	S_{c1}	S_{c2}
Nominal	20.2	1.67	$6.89e6$	2.28	$1.06e-3$
ID 2667	19.8	1.48	$1.27e7$	2.01	$8.38e-4$
ID 2430	15.0	1.68	$7.17e6$	2.21	$9.86e-4$

TABLE III

Design characteristics of optimal solutions.

Parameters (Unit)	Nominal	ID 2667	ID 2430
$L_1\ (m)$	0.75	0.743	0.746
$L_2\ (m)$	0.95	0.961	0.942
$L_3\ (m)$	0.125	0.112	0.106
$T_1\ (mm)$	5	5	2
$T_2\ (mm)$	2	3	2
$\phi_1\ (mm)$	70	88	98.5
$\phi_2\ (mm)$	28	18.5	17
$\phi_3\ (mm)$	22	22	25.5
$R_n\ (m)$	0.2	0.161	0.177

TABLE IV

Mean and maximum of the TCP elastic displacements.

Design	$\delta x_i(mm)$		$\delta y_i(mm)$		$\delta z_i(mm)$	
	mean	max	mean	max	mean	max
Nominal	-0.006	2.28	0.0	3.93	1.80	3.17
ID 2667	-0.003	1.18	0.0	1.98	0.94	1.68
ID 2430	-0.007	1.99	0.0	3.62	1.65	2.85
Design	$\delta\theta x_i(mrad)$		$\delta\theta y_i(mrad)$		$\delta\theta z_i(mrad)$	
	mean	max	mean	max	mean	max
Nominal	0.0	8.86	-0.01	6.79	0.0	0.42
ID 2667	0.0	5.97	-0.01	4.38	0.0	0.27
ID 2430	0.0	8.35	-0.01	5.90	0.0	0.49

[2] J. Duffy. *Statics and kinematics with applications to robotics*. Cambridge University Press, 1996.

[3] K. Shroer, S. L. Albright, and A. Lisounkin. Modeling closed-loop mechanisms in robots for purposes of calibration. *IEEE Trans. on Rob. and Aut.*, 13(2):218–229, 1997.

[4] M. Damak and J. Grosbois. Vision robot based absolute accuracy measurement. In *ISR 2004*, Paris, France, 2004.

[5] G. Alici and B. Shirinzadeh. Enhanced stiffness modeling, identification and characterization for robot manipulators. *IEEE Trans. on Rob. and Aut.*, 21(4):554–564, 2005. 1552-3098.

[6] S. Marie and P. Maurine. Elasto-geometrical modelling of closed-loop industrial robots used for machining applications. In *IEEE Int. Conf. on Rob. and Aut., 2008*, pages 1294–1300, 2008.

[7] G. Carbone and M. Ceccarelli. A comparison of indices for stiffness performance evaluation. In *IFToMM'07*, Besançon, France, 2007.

[8] C. Gosselin and SA INRIA. Stiffness mapping for parallel manipulators. *IEEE Trans. on Rob. and Aut.*, 6:377–382, 1990.

[9] G. J. Wiens and D. S. Hardage. Structural dynamics and system identification of parallel kinematic machines. In *2006 ASME Int. Design Engineering Technical Conf. & Computers and Information in Engineering Conf., Philadelphia, Pennsylvania, USA*, 2006.

[10] M. Krefft and J. Hesselbach. Elastodynamic optimization of parallel kinematics. *IEEE Int. Conf. on Aut. Science and Engineering*, pages 357–362, 2005.

[11] S. D. Stan, V. Maties, and R. Balan. Genetic algorithms multiobjective optimization of a 2 dof micro parallel robot. *IEEE Conf. on Emerging Technologies & Factory Aut.*, pages 780–783, 2007.

[12] R. Unal, G. Kiziltas, and V. Patoglu. A multi-criteria design optimization framework for haptic interfaces. *Symposium on Haptic Interfaces for Virtual Environment and Teleoperator Systems*, pages 231–238, 2008.

[13] D. Deblaise, X. Hernot, and P. Maurine. A systematic analytical method for pkm stiffness matrix calculation. In *IEEE Int. Conf. on Rob. and Aut.*, pages 4213 – 4219, Orlando, Floride, USA, 2006.

[14] J. P. Merlet. Jacobian, manipulability, condition number, and accuracy of parallel robots. *Journal of Mechanical Design*, 128:199–206, 2006.

[15] *modeFRONTIER: http://www.esteco.com.*

[16] R. Clavel. Delta, a fast robot with parallel geometry. In *18th Int. Symp. Ind. Robots*, pages 91–100, Lausanne, Switzerland, Apr. 1988.

[17] H. S. Kim. *Design and control of a Stewart platform based machine tool*. Ph.d. thesis, Yonsei University, Korea, 1999.

[18] M. Griffis and J. Duffy. Kinestatic control: A novel theory for simultaneously regulating force and displacement. *Journal of Mechanical Design*, 113:508, 1991.

[19] H. Lipkin and T. Patterson. Geometrical properties of modeled robot elasticity: Part I Decomposition. In *1992 ASME Design Technical Conf., Scottsdale, DE*, volume 45, pages 179–185, 1992.

[20] Raffaele Di Gregorio. Determination of singularities in delta-like manipulators. *The Int. Journal of Rob. Research*, 23:89–96, 2004.

[21] F. Majou, C. Gosselin, P. Wenger, and D. Chablat. Parametric stiffness analysis of the orthoglide. *Mechanism and Machine Theory*, 42:296–311, 2007.

[22] C. M. Fonseca and P. J. Fleming. Multiobjective optimization and multiple constraint handling with evolutionary algorithms. *IEEE Trans. on Systems, Man, and Cybernetics*, 28:26–37, 1998.

[23] A. Inselberg, B. Dimsdale, IBMS Center, and C. A. Los Angeles. Parallel coordinates: a tool for visualizing multi-dimensional geometry. *IEEE Conf. on Visualization*, pages 361–378, 1990.